Calculation on the Band Structure of GaAs using $k \cdot p$ -theory FFF042

I-Ju Chen, Sara Thorberg, Yang Chen

December 17, 2014

1 Introduction

With its superior electronics and optical characteristics, GaAs is easily the most commonly used III−V material for electronics and optoelectronics. GaAs has a higher electron mobility and less noise compared to Si, therefore it is used to make high-frequency transistor, phone and satellite communication circuitry, and high frequency radar system [1]. In addition, the band gap of GaAs is in the infrared, which is advantageous for optoelectronic applications. GaAs-based device holds the highest record for the highest efficiency single-junction solar cell [2]. Furthermore, GaAs is used in the manufacture of infrared light-emitting diodes (LEDs) [3], which are used in optical communications and control systems.

Recently an upsurge of new and interesting nanowire structures has also been realized based on GaAs. In its bulk state, GaAs is stable in the zinc-blende structure. When reduced to the nanoscale, such as in the form of nanowires, wurtzite structure becomes stable. In this way, pure wurtzite phase GaAs and zinc-blende/wurtzite GaAs heterostructures have been realized. Wurtzite and Zincblende crystals possess very distinguished band structures. Therefore, the success to grow wurtzite GaAs crystal has brought the possibilities to create new devices, such as a device that can simultaneously serve as LED and photodetector [3], and to build GaAs 'heterostructures' with the two different crystal phase.

Therefore it is of interest to study the electronic band structure of wurtzite GaAs. Experimentally, photoluminescence and Raman spectroscopy have been applied to study single crystal wurtzite GaAs [3],[4]. On the other hand, multiple calculation methods including empirical pseudopotentials [5], full-potential linearized muffin-tin orbital method (FP-LMTO)[6], and density-functional theory in the local density approximation (LDA) [7] have all been applied to calculate the band-structure of GaAs wurtzite crystal. Moreover, the GaAs wurtzite-zincblende heterostructure nanowires have also been investigated with various experimental technique, including cathodoluminescence, photoluminescence [8], Raman spectroscopy, and time-resolved luminescence [9]. Here we used k.p method as a common approach to calculate the band structure of GaAs zinc blende and wurtzite crystal. It has the advantage of the simplicity to apply to low-dimension and heterostructure.

2 $k \cdot p$-theory

The $k \cdot p$-theory is a multi-band approximation which means that contributions from several bands are considered in the calculations. The calculation would be completely accurate if an infinite number of bands were used, however, it is not necessary for high accuracy. Even a low number of bands are sufficient to obtain structures which are correct for a certain region of interest. In this project, eight bands have been calculated and the remaining bands were considered as perturbations. Focus was on the region around the Γ point, i.e. the mid point of the Brillouin zone, $\boldsymbol{k} = 0, 0, 0$, where the free charge carriers are confined in semiconductors, such as GaAs and GaN.

The $k \cdot p$ presentation is obtained when inserting the periodic wave function (equation1) into the Hamiltonian for a single electron in a periodic potential V_{per} (equation 2). This is described by Davies [10] and Kane [11].

$$\psi_k = \exp(i\boldsymbol{k} \cdot \boldsymbol{p}) u_k(\boldsymbol{r}) \tag{1}$$

$$H = -\frac{\hbar^2}{2m_0}\nabla^2 + V_{per}(\boldsymbol{r}) \tag{2}$$

The resulting Hamiltonian is shown below in equation 3, where the first two terms are independent of $\boldsymbol{k}$ and the second two terms are dependent of $\boldsymbol{k}$.

$$\left[\frac{p^2}{2m_0} + V_{per}(\boldsymbol{r}) + \frac{\hbar}{m_0}\boldsymbol{k} \cdot \boldsymbol{p} + \frac{\hbar^2 k^2}{2m}\right] u_{nk}(\boldsymbol{r}) = E_n(\boldsymbol{k}) u_{n\boldsymbol{k}}(\boldsymbol{r}) \tag{3}$$

The energy can be expanded using Löwdin perturbation theory which uses both perfect diagonalization of the Hamiltonian and perturbation theory of the remaining states. For a single band, this treatment results in equation 4 (second order perturbation) for the region around $\boldsymbol{k} = \boldsymbol{0}$ [10]. The last term in the equation is the diagonal matrix elements.

$$E_n(\boldsymbol{k}) = E_n(\boldsymbol{0}) + \frac{\hbar}{m_0}\boldsymbol{k} \cdot \boldsymbol{p_{nn}} + \frac{\hbar^2 k^2}{2m_0} + \frac{\hbar^2}{m_0^2}\sum_{n'} \frac{|\langle m\boldsymbol{0}| \boldsymbol{k} \cdot \hat{\boldsymbol{p}} |n\boldsymbol{0}\rangle|^2}{E_n(\boldsymbol{0}) - E_{n'}(\boldsymbol{0})} \tag{4}$$

2.1 Zincblende

One of the crystals investigated in this project is the zincblende. The Zincblende crystal structure and the Weigner-Seitz cell of the first Brillouin zone is illustrated in figure 1. In figure 1(b) different positions in the first Brillouin zone is marked, e.g. the origin is labeled Γ.

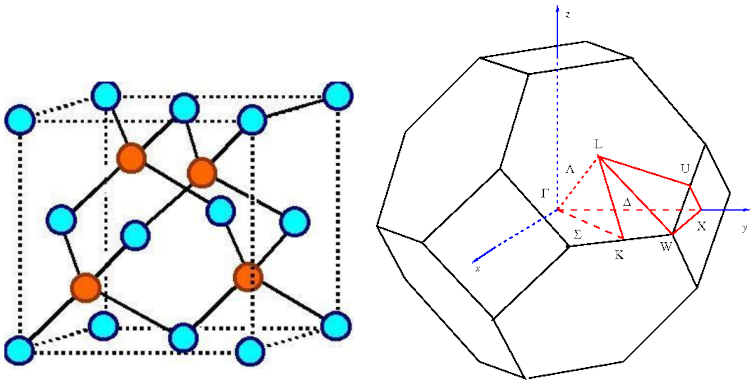

(a) Crystal structure. (b) First Brillouin zone.

Figure 1: Strucure of the crystal and the first Brillouin zone for zincblende, [13].

The 8 × 8 Hamiltonian matrix (5) includes the conduction band and the three valence bands[16].

$$H = \begin{bmatrix} G & \Gamma \\ -\Gamma^* & G^* \end{bmatrix} \tag{5}$$

Each element in the Hamiltonian matrix are 4×4 matrices. G is the interaction term and is given by the sum: $G(\boldsymbol{k}) = G_1(\boldsymbol{k}) + G_2(\boldsymbol{k}) + G_{so}$, where:

$$G_1 = \begin{bmatrix} E_c & iPk_x & iPk_y & iPk_z \\ -iPk_x & E_{\nu'} & 0 & 0 \\ -iPk_y & 0 & E_{\nu'} & 0 \\ -iPk_z & 0 & 0 & E_{\nu'} \end{bmatrix} \tag{6}$$

$$G_2 = \begin{bmatrix} A'k^2 & Bkyk_z & Bk_xk_z & Bk_xk_y \\ Bk_yk_z & L'k_x^2 + M(k_y^2 + k_z^2) & N'k_xk_y & N'k_xk_z \\ Bk_zk_x & N'k_xk_y & L'k_y^2 + M(k_x^2 + k_z^2) & N'k_yk_z \\ Bk_xk_y & N'k_xk_z & N'k_yk_z & L'k_z^2 + M(k_x^2 + k_y^2) \end{bmatrix} \tag{7}$$

$$G_{so} = -\frac{\Delta}{3} \begin{bmatrix} 0 & 0 & 0 & 0 \\ 0 & 0 & i & 0 \\ 0 & -i & 0 & 0 \\ 0 & 0 & 0 & 0 \end{bmatrix} \tag{8}$$

$$\Gamma = -\frac{\Delta}{3} \begin{bmatrix} 0 & 0 & 0 & 0 \\ 0 & 0 & 0 & -1 \\ 0 & 0 & 0 & i \\ 0 & 1 & -i & 0 \end{bmatrix} \tag{9}$$

$B = 0$ due to symmetry of the crystal around the Γ point. The spin-orbit interaction is included through G_{so} in equation 8 where Δ is the spin-orbit splitting.

2.2 Wurtzite

Wurtzite structure is the reciprocal lattice of zincblende structure. So they share the same symmetry in lattice group theory. [14] The crystal structure is shown in figure 2.

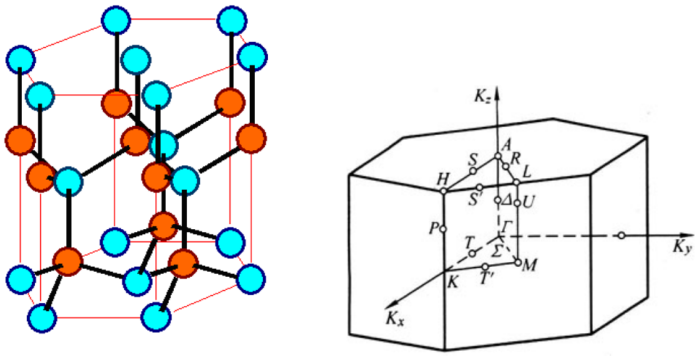

(a) Crystal structure. (b) First Brillouin zone.

Figure 2: Strucure of the crystal and the first Brillouin zone for wurtzite, [13].

In general, the matrix of G_1 and G_2 have the similar form compared with zincblende case. In Ref. [15], six-band model is introduced to this problem. Here we only give the final eight-band hamiltonian matrix directly.

$$H_w = \begin{bmatrix} E_c + \frac{\hbar^2 k^2}{2m_0} & x_1 & x_2 & x_3 & 0 & 0 & 0 & 0 \\ -x_2 & F & -K^* & -H^* & 0 & 0 & 0 & 0 \\ -x_1 & -K & G & H & 0 & 0 & 0 & \Delta \\ x_3 & H & -H^* & \lambda & 0 & 0 & \Delta & 0 \\ 0 & 0 & 0 & 0 & E_c + \frac{\hbar^2 k^2}{2m_0} & x_2 & x_1 & x_3 \\ 0 & 0 & 0 & 0 & -x_1 & F & -K & H \\ 0 & 0 & 0 & \Delta & -x_2 & -K^* & G & -H^* \\ 0 & 0 & \Delta & 0 & x_3 & H^* & -H & \lambda \end{bmatrix} \tag{10}$$

where $x_1 = -\frac{(k_x+ik_y)P_2}{\sqrt{2}}$, $x_2 = \frac{(k_x-ik_y)P_2}{\sqrt{2}}$ and $x_3 = k_z P_1$. Here we use the same symbols with Ref. [15] and all the parameters undefined here can be found in Ref. [15].

But we should notice that in both cases, we take the same approximation which $B = 0$ in G_2. In general, $B = 0$ means the crystal has a inversion symmetry [16]. Actually for both zencblende and wurtzite crystal, they do not have a strict inversion symmetry. It can be seen clearly in Figure 1 and 2. It is used in [16] and [15] as B is very small.

The only remaining problem is to calculate the eigenvalues of this Hamiltonian by Secular equation

$$det \mid H - EI \mid = 0$$

2.3 Parameters

This section include the parameters used in the matrices and equation in the previous sections. These parameters are summarized in table 1.

	Zincblende		Wurtzite
E_g (eV)	1.424 [16]	E_g (eV)	1.503 [5]
a_0 (Å)	5.653 [16]	a_0 (Å)	4.050 [6]
Δ (eV)	0.331	Δ_{cr} (eV)	0.244 [5]
m_e	0.0665	Δ_{so} (eV)	0.351 [5]
A'	$2.29 \cdot 10^{-17}$ [16]	m_e^z	0.060 [6]
L'	$3.006 \cdot 10^{-38}$[16]	m_e^t	0.075 [5]
N'	$2.275 \cdot 10^{-38}$[16]	A_1	18.39 [6]
M	$-2.388 \cdot 10^{-38}$ [16]	A_2	1.87 [6]
P	$1.681 \cdot 10^{-28}$ [17]	A_3	17.05 [6]
		A_4	6.26[6]
		A_5	6.83[6]
		A_6	7.27[6]

Table 1: Parameters for zincblende and wurtzite GaAs.

3 Numerical Results

In this part, the resulting energy bands for the different calculations are presented. In the plots the positive x-axis shows the energy bands in the k_x-direction and the negative x-axis in the k_z-direction. This is to clearly show the similarities and the differences in the different directions.

Figure 3 show the energy bands of the zincblende GaAs. The valence band split into three subband: heavy-hole band , light-hole band and spin-orbit splitting band from top to down[15] [16]. Each band has a degeneracy of two as there are two electrons on the same energy level. Total number of conduction band and valence band is equal to the dimension of hamiltonian matrix.

In the same figure, two percent compression is imposed in the system. It can be seen from the dotted line that the energy gap increases and the major line shape is still parabolic like without changing for each band. But heavy and light hole degeneracy is gone as a small energy difference occurs at Γ point. In the zincblende GaAs case, $k \cdot p$ pertubation part in energy is relatively small.

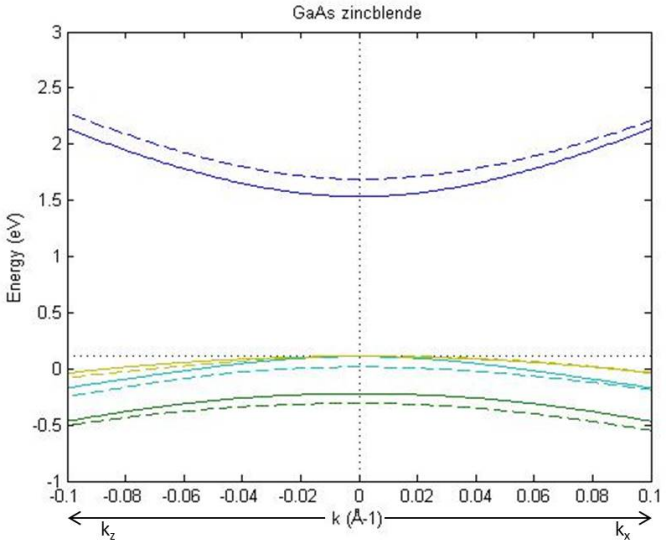

Figure 3: Energy levels for zincblende GaAs. Unstrained crystal plotted with solid lines and 2 % strained crystal plotted with dashed lines.

$k \cdot p$ pertubation part is stronger in wurtzite GaAs case. It can be seen clearly in Figure 4 that along k_x direction the line shapes of heavy and light hole band change significantly. Another difference in wurtzite GaAs is that even without straining wurtzite GaAs also splits at Γ point for heavy and light hole bands. It will lead to some fundamental differences in their electric and optical properties[15]. At the same time, the band gaps for zincblende and wurtzite GaAs are approximately the same.

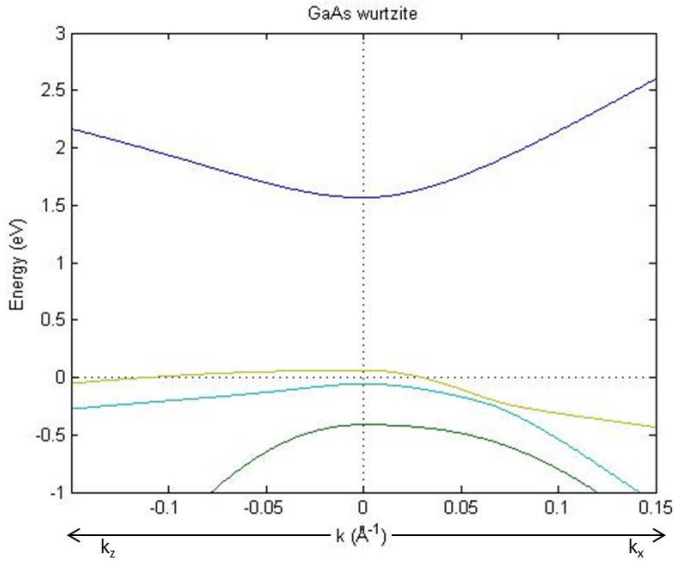

Figure 4: Energy levels for wurtzite GaAs.

At last, eight-band structure of GaN is calculated and shown in Figure 5. As the band gap of GaN is more than 3 eV which is too large compared with its valence band splitting energy around 0.01 eV, we do not plot conduction band in this figure. It can be seen from k_x direction that band shape deformation is stronger in GaN than GaAs. But along k_z direction for both GaN and GaAs we do not see this kind of deformation.

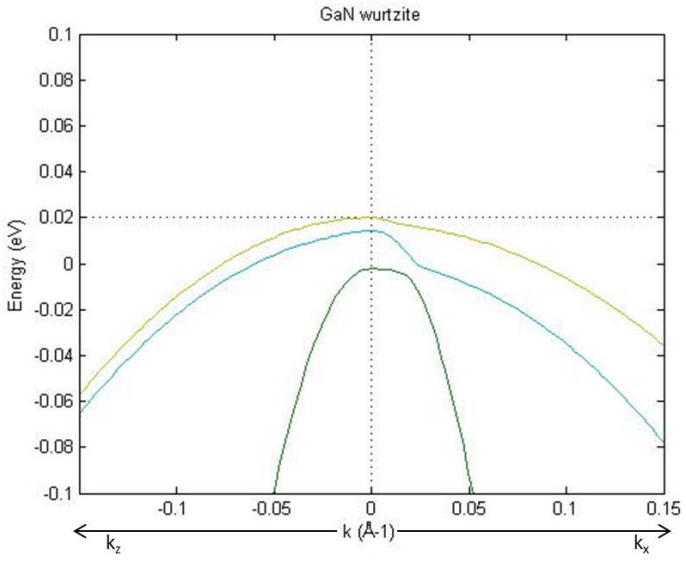

Figure 5: Energy levels for wurtzite GaN.

4 Discussion

Moreover, we can also observe some interesting difference between the electronic band structures of ZB and WZ GaAs. First of all, WZ and ZB GaAs crystal has very similar band gap. Secondly, the electron band energies are around 60 meV higher in WZ GaAs compare to ZB GaAs. It can explain the type-II heterojunction that was observed at GaAs ZB-WZ interface [8]. Moreover, in contrast to ZB phase, the valence band of WZ GaAs splits in three bands heavy hole (HH band), light-hole (LH band), and crystal-filed-split-off (CH band)) as a combination of spin-orbit and crystal field splitting. The crystal field split energy is exclusively added to the simulation of WZ crystal band structure because of the anisotropy of the wurtzite symmetry. It represents the difference between the expectation value of the unperturbed periodic potential of the X-like/ Y-like state and Z-like state before spin-orbit coupling effect is considered. Finally, we can also observe that the band structure of WZ GaAs exhibit a greater difference between the k_x and k_z direction relative to ZB GaAs. It is a result of the anisotropy of the WZ crystal structure.

5 Conclusion

In this report, we use $k \cdot p$ pertubation theory to investigate the band structure of materials. Zincblende GaAs and wurtzite GaN and GaAs are considered in an eight-band model. The ZB GaAs crystal is highly symmetric around Γ which leads to symmetric energy bands around Γ. The energy bands for the light and heavy holes are also degenerate, however, this degeneracy is broken when strain is imposed on the crystal. The compressive strain leads to an increase in the bandgap, and since the strain is applied in the x-direction, the energy bands are no longer the same in the different directions. The anisotropy of the wurtzite crystal shows in the energy bands. Both in the WZ GaAs and in the WZ GaN the energy bands take on a different form in the x-direction compared to the z-direction. The difference in the energy bands for the WZ GaAs compared to the ZB GaAs means that the two crystals will have different electronic properties and thus be used for diffent applications.

References

[1] Fisher, D.G., Bahl, I.J. (1995). *Gallium arsenide IC applications handbook.* San Diego: Academic Press.

[2] *NREL Reports 31.1% Efficiency for III-V Solar Cell* NREL: News -. 24 June 2013. Web. 16 Dec. 2014.

[3] Signorello, G. et al. (2014) *Inducing a direct-to-pseudodirect bandgap transition in wurtzite GaAs nanowires with uniaxial stress.* Nat. Commun. 5, 3655.

[4] Ketterer, Bernt. (2011) *Determination of the Band Gap and the Split-off Band in Wurtzite GaAs Using Raman and Photoluminescence Excitation Spectroscopy.* Physical Review B 83, 12.

[5] De, A., & Pryor, C. (2010). *Predicted band structures of III-V semiconductors in the wurtzite phase.* Physical Review B, 81, 155210-155210.

[6] Cheiwchanchamnangij, T., & Lambrecht, W. (2011). *Band structure parameters of wurtzite and zinc-blende GaAs under strain in the GW approximation.* Physical Review B, 84, 035203-035203.

[7] Murayama, M., & Nakayama, T. (1994). *Chemical trend of band offsets at wurtzite/zinc-blende heterocrystalline semiconductor interfaces.* Physical Review B, 49(7), 4710-4724.

[8] Vainorius, Neimantas. *Observation of Type-II Recombination in Single Wurtzite/zinc-blende GaAs Heterojunction Nanowires.* PHYSICAL REVIEW B 89, 165423 (2014)

[9] Spirkoska, D. (2009). *Structural and optical properties of high quality zinc-blende/wurtzite GaAs nanowire heterostructures.* Physical Review B, 80, 245325-245325.

[10] Davies, J. H., (1997). *The Physics of Low-dimensional Semiconductors - An Introduction.* Cambridge University Press.

[11] Kane, E.O. (1982). "Energy Band Theory", in *Handbook on Semiconductors*, vol 1, Paul, W. Ed. Amterdam, North Holland, pp. 193-217.

[12] Ehrhardt, M., Koprucki, T. (2014). *Multi-Band Effective Mass Approximation.* Springer Verlag, Heidelberg.

[13] Föll, H. (Semiconductor Technilogy -Script) `http://www.tf.uni-kiel.de/matwis/amat/semitech_en/index.html`, retrieved December, 15, 2014.

[14] Christopher Bradley and Arthur Cracknell *The Mathematical Theory of Symmetry in Solids.* Oxford University Press, USA, 2010. Print.

[15] S. L. Chuang and C. S. Chang, $k \cdot p$ *method for strained wurtzite semiconductors.* Physical Review B 54, 2491 (1996)

[16] D. Gershoni, C. H. Henry and G. A. Baraff, *Calculating the Optical Properties of Multidimensional Heterostructures: Application to the Modeling of Quaternary Quantum Well Lasers.* IEEE Journal of Quantum Electronics, 29, 2433 (1993)

[17] Winkler, R. (2003). *Spin-Orbit Coupling Effects in Two-Diemnsional Electron and Hole Systems.* Springer.